

NUMERICAL PROPAGATION SIMULATIONS AND COHERENCE ANALYSIS OF SASE WAVEFRONTS*

O. Chubar[#], M.-E. Couprie, F. Polack, SOLEIL, 91191 Gif-sur-Yvette, France
M. Labat, G. Lambert, O. Tcherbakoff, CEA, DSM/SPAM, 91191 Gif-sur-Yvette, France

Abstract

Examples of wavefront propagation simulation and coherence analysis of Self-Amplified Spontaneous Emission (SASE), seeded and started-up from noise, are presented. The calculations are performed using SRW – the wave-optics computer code optimized for Synchrotron Radiation (SR), and the 3D FEL simulation code GENESIS. To ensure easy inter-operation and data exchange between the two codes, GENESIS has been integrated into the “emission” part of the SRW, which is dedicated for calculation of initial wavefronts in the form ready for subsequent propagation simulations. After each run of GENESIS in time-dependent mode, the resulting electric field is transformed from time to frequency domain, and the wavefront obtained this way is numerically propagated, using Fourier-optics methods implemented in SRW, from the exit of FEL undulator to a destination plane of a beamline containing several optical elements separated by drift spaces. Interferometer-type optical schemes, which allow for “probing” spatial and temporal coherence of SASE wavefronts, are used in the examples. Intensity distributions of the propagated radiation are extracted and analysed in time and frequency domains. The presented examples show that the SRW code can be used for optimization of optical beamlines for 4th generation synchrotron radiation sources, which require accurate treatment of wave-optical phenomena in frequency and time domains.

INTRODUCTION

Synchrotron Radiation emitted by relativistic electrons in magnetic fields of storage ring sources of the 3rd generation is a proven tool for research in many areas of science, from physics and chemistry to biology and medicine. An outstanding feature of the SR is a very broad emission spectrum extending from far infrared to hard X-ray range. Besides, undulator-based 3rd generation SR sources offer relatively high average spectral flux, brightness and degree of spatial coherence of the output radiation, and a possibility to use this radiation simultaneously for various experiments at a large number of beamlines.

The new emerging sources of the 4th generation – free-electron lasers and energy-recovery linacs – extend the domain of SR applications to time-resolved research, by providing femtosecond and, prospectively, even attosecond time scale pulses of radiation with extremely high peak brightness [1, 2].

To fully exploit all great SR features in the 3rd and 4th generation sources, high-accuracy simulation tools for the

processes of emission and wavefront propagation through various optical elements of a beamline should be used. In the frame of classical electrodynamics, such simulation tools, dedicated both for the emission and propagation parts, would operate with 3D electric field of radiation [3]. Whereas this requirement seems absolutely natural for the emission part, it is much less evident for the propagation, where simple geometrical optics based approximation exists and is extensively (and successfully) used for incoherent sources and systems dominated by optical aberrations. Nevertheless, with decrease of electron beam emittance in storage rings [4] and continuous progress in the quality of optical elements [5-7], the radiation gradually approaches diffraction limit for shorter and shorter wavelengths, making physical-optics approaches to simulation of wavefront propagation increasingly important.

Two physical-optics based approaches to wavefront propagation simulation are currently popular: Fourier optics [8] and asymptotic expansions (mainly, the stationary phase method) [9, 10]. This paper deals with the Fourier optics approach, as it is implemented in the SRW computer code [11, 12].

The following are proven “strong points” of the Fourier optics method:

- very high CPU efficiency;
- possibility to take into account multiple diffractive/ refractive/ reflective optical elements in “uniform” way without any increase of the overall complexity;
- stability in case of “noisy” wavefronts (these methods are extensively used for simulation of scattering);
- availability of large amount of data on electric field after only one propagation pass.

Among “weak points” of this method one can mention:

- large amount of memory required for “standard” near-field propagator through free space, and
- poor accuracy of the “thin” element approximation for simulating grazing incidence optics and/or optics with very wide angular apertures.

We note that for the 3rd generation sources, it is often enough to simulate wavefront propagation through a beamline only in frequency domain – at one central or eventually at several different frequencies / photon energies. On the other hand, the 4th generation sources require a combined frequency- and time-domain analysis because of the necessity to preserve (or at least to keep track of) temporal characteristics of propagating wavefronts. To profit of CPU efficiency of the Fast Fourier Transforms (FFT), which are used by the free-space propagator and at changing the electric field representation between the frequency and time domains, it is preferable to keep in memory at each step of

*Work supported by EuroFEL

[#]oleg.chubar@synchrotron-soleil.fr

propagation an entire “instant” wavefront, meshed not only vs two transverse coordinates, but also vs frequency (or time). This makes the memory constraint even more important. In the following sections, we show that despite of this constraint, the Fourier optics method can be very efficiently used for simulating propagation of time-dependent SASE wavefronts produced by FELs.

BRIEF METHOD DESCRIPTION

Time- and Frequency-Domain Representations

Time- and frequency-domain complex electric fields $\vec{E}(\vec{r}, t)$ and $\vec{E}(\vec{r}, \omega)$ are well known to be related by the Fourier transform:

$$\begin{aligned}\vec{E}(\vec{r}, \omega) &= \int_{-\infty}^{\infty} \vec{E}(\vec{r}, t) \exp(i\omega t) dt \\ \vec{E}(\vec{r}, t) &= \frac{1}{2\pi} \int_{-\infty}^{\infty} \vec{E}(\vec{r}, \omega) \exp(-i\omega t) d\omega\end{aligned}\quad (1)$$

where t is time, ω is cyclic frequency (linked to photon energy via the reduced Planck constant $\varepsilon = \hbar\omega$), \vec{r} is observation point.

Initial SASE wavefronts are often calculated in time domain [13]; however, propagation of the electric field in free space or in media is described in the frequency domain [14]. Besides, it is often necessary to follow the evolution of both temporal and spectral characteristics of a wavefront at different propagation steps. It is therefore important to use an efficient algorithm for Eq. (1). Such algorithm can be based on a prime-factor FFT [15], which would be applied “in place” to a “flat” (or “C-aligned”) complex electric field data structure – for many space points \vec{r} in parallel.

Fourier-Optics Propagators

The propagation of transverse components of the frequency-domain electric field in free space is well known to be described by the Huygens-Fresnel principle, which, for small emission and observation angles is [14]:

$$\vec{E}_{\perp}(\vec{r}_2, \omega) \approx \frac{-i\omega}{2\pi c} \iint_{\Sigma_1} \vec{E}_{\perp}(\vec{r}_1, \omega) \frac{\exp[i\omega|\vec{r}_2 - \vec{r}_1|/c]}{|\vec{r}_2 - \vec{r}_1|} d\Sigma_1 \quad (2)$$

where the integration is performed over surface Σ_1 ; \vec{r}_1 is point on that surface (varying at the integration), \vec{r}_2 is an observation point, c is speed of light. If Σ_1 is a plane, e.g. perpendicular to Z axis, and \vec{r}_2 belongs to another plane, located at distance Δz from Σ_1 , then $d\Sigma_1 = dx_1 dy_1$, $|\vec{r}_2 - \vec{r}_1| = [\Delta z^2 + (x_2 - x_1)^2 + (y_2 - y_1)^2]^{1/2}$, and Eq. (2) is a convolution-type integral, which can be quickly calculated using 2D FFT.

In practice, direct application of the convolution theorem to Eq. (2) for the case of propagation between parallel planes may result in the necessity of very dense sampling of the electric field vs transverse coordinates x_1 and y_1 (and/or x_2, y_2), because the phase of the field at

some distance from source depends quadratically on these coordinates and all oscillations of the field within given wavefront limits must be resolved (otherwise accuracy may be lost). There are several possibilities to walk around this problem. One consists in distinguishing more economic (in terms of sampling) “special cases” of propagation, such as propagation to or from waist, when Eq. (2) can be reduced to one Fourier transform and multiplication of the field by phase factors which depend on the transverse coordinates.

More generally, if approximate values of wavefront radii and centres with respect to transverse coordinates are known, one can “subtract” the quadratic phase terms from the initial wavefront; then, within the quadratic phase approximation, Eq. (2) can still be reduced to a convolution, with the necessity to re-scale (and eventually shift) the resulting wavefront, and add a new (modified) quadratic phase term to it. This simple manipulation can dramatically reduce the amount of memory required for the propagation, while preserving high efficiency and accuracy of the Fourier optics method.

Electric field transformation at propagation from a transverse plane before an optical element (e.g. lens, mirror, aperture, zone plate, grating,...) to a plane immediately after it can be formally represented as:

$$\begin{aligned}\vec{E}_{\perp out}(x_2, y_2, \omega) &\approx \mathbf{G}(x_2, y_2, \omega) \exp[i\omega L(x_2, y_2)/c] \times \\ &\times \vec{E}_{\perp in}(x_1(x_2, y_2), y_1(x_2, y_2), \omega)\end{aligned}\quad (3)$$

where, in general case, $\mathbf{G}(x_2, y_2, \omega)$ is a 2x2 matrix function of the output transverse coordinates and frequency, which can take into account eventual anisotropy of the optical element with respect to transverse components of the input electric field; the optical path function $L(x_2, y_2)$ and the input/output coordinate transformation $x_1(x_2, y_2), y_1(x_2, y_2)$ can be deduced from geometrical optics, or by applying the stationary phase method. We note that for a “thin” optical element, Eq. (3) is reduced to simple multiplication of the input field by a complex transmission function.

Wavefront Resizing and Resampling

Transverse dimensions and/or oscillation rates of electric field may strongly vary during the propagation. In order to keep the electric field sufficiently well dimensioned and resolved at each step of the propagation (as required by the propagators being used to simulate optical elements and free spaces) and, at the same time, stay within reasonable memory consumption, efficient mechanisms of wavefront resizing (changing limits) and resampling (changing steps of the grid) should be used. The resampling can be performed either by using interpolation, or by applying FFT and resizing the electric field on the Fourier side. E.g., if there is a necessity to decrease step of transverse position(s), one can perform forward FFT and increase limit(s) by padding zeros on the Fourier side, and then perform backwards FFT. At manipulations with time-dependent wavefronts, the use of

the resizing and resampling procedures is particularly important, and it should be used not only to transverse coordinates (/angles), but also for time (/frequency).

APPLICATIONS FOR TIME-DEPENDENT SASE WAVEFRONTS

To illustrate application of the Fourier-optics based method, as it is implemented in the SRW code, for simulating propagation of time-dependent SASE wavefronts, we use two simple interference-type optical schemes, one of them being sensitive to spatial, and the other one to temporal coherence of an input wavefront. Of course, the range of potential applications of the method is not limited by these types of optical schemes.

Two different wavefronts are numerically propagated through the optical schemes: (almost fully) saturated radiation wavefront obtained at seeded FEL operation and a wavefront of unsaturated SASE.

All calculations described in this section were performed on a regular laptop PC with 1 GB of memory under 32-bit Windows. In all considered cases, the simulation of wavefront propagation took small amount of CPU time (in the range of minutes) compared to the calculation of initial time-dependent wavefronts.

Wavefronts at FEL Exit

The two initial wavefronts were calculated using GENESIS (integrated into SRW) for the parameters corresponding to the phase 2 of the ArcEnCiel project [16]:

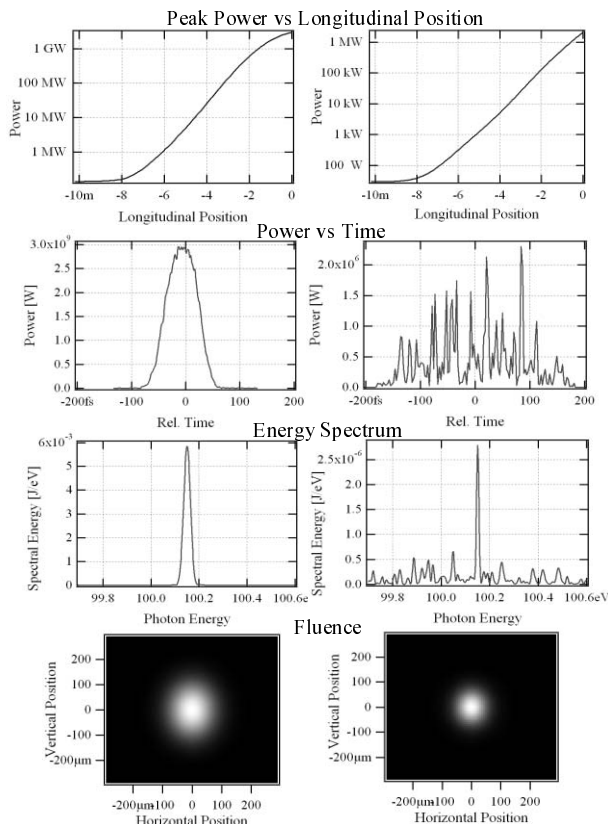


Figure 1: Radiation characteristics at FEL exit for two cases: seeded (left) and started up from noise (right).

FEL Theory

electron beam at 1 GeV energy, 1.5 kA peak current, 60 μm RMS bunch length, 1.2π mm-mrad normalized emittance; planar undulator with 30 mm period and deflecting parameter ~ 2.06 , composed out of five 2 m long sections. In one case, a seeding radiation pulse of 50 kW peak power and 22 fs RMS duration, at 100.15 eV average photon energy was used (the seed was assumed to be produced by the process of generation of high harmonics in gas [17]). In the other case, no external seed was applied. The results of time-dependent calculations (peak power, pulse profile, energy spectrum, fluence/intensity distribution at FEL exit) obtained for the two cases are presented in Fig. 1.

Young's Double-Slit Interferometer

The Young's double-slit interferometer scheme, shown in Fig. 2, allows one to test transverse coherence of input radiation [14].

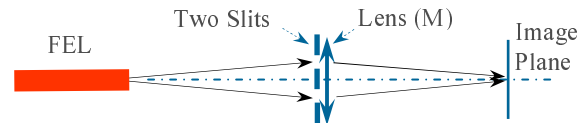


Figure 2: Double-slit interferometer scheme.

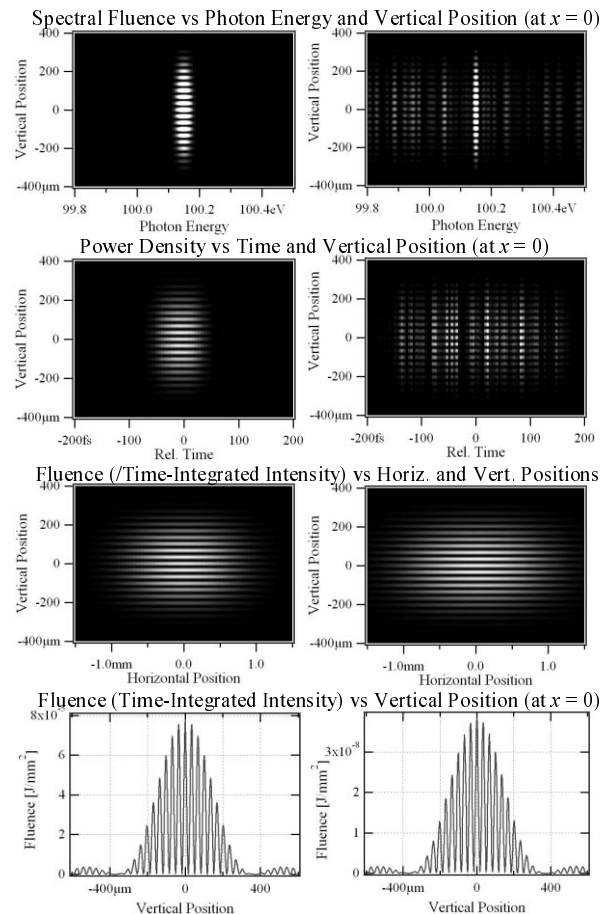


Figure 3: Wavefront characteristics in the image plane of double-slit interferometer scheme for two FEL regimes: seeded (left) and started up from noise (right).

The following parameters of this scheme were used for SASE wavefront propagation calculations: 20 m distance from the FEL exit to the slits, 1 mm vertical distance between the slits, 0.1 mm slit widths, 2.6 m/18 m vertical/horizontal focal distance of an astigmatic lens (mirror), and 3 m distance from the lens to the image plane. The calculation results obtained for the image plane in the two wavefront cases (as described above) are presented in Fig. 3. One can see that in both cases, the visibility of interference fringes, characterizing the degree of spatial coherence, is ~ 1 .

Double-Slit Interferometer with Grating

A simple scheme for probing temporal coherence can be obtained by inserting a grating into the double-slit interferometer, just before (or immediately after) the slits and the mirror, as shown in Fig. 4.

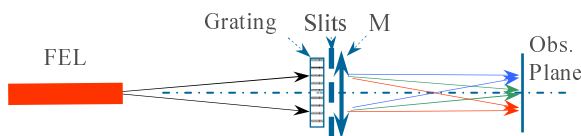


Figure 4: Double-slit interferometer with grating.

Simulation results on wavefront propagation to the observation plane for the two cases of input SASE are illustrated in Fig. 5. At this calculation, the vertical and horizontal focal distances of the mirror were 3.7 m and 100 m; the observation plane was at ~ 3.8 m from the mirror. The grating was assumed to be flat, with groove density of 150 l/mm; the incidence angle $\sim 2.5^\circ$ (in vertical plane).

We see from Fig. 5 that for both wavefront cases, the interference patterns are strongly modified by the grating. Vertical positions of interference peaks depend now on photon energy (see upper image plots), and this reduces the visibility of fringes in the resulting frequency- (or time-) integrated patterns. As one can see from the graphs, the poor visibility of fringes in the seeded case has also simple time-domain interpretation: because of the delay introduced by the grating, the radiation pulses from the two slits almost don't overlap in time.

We note that in the case of SASE started from noise, the interference pattern depends on pulse micro-structure (having stochastic origin) and can therefore appear further "smoothed-out" after averaging over ensemble of pulses. The corresponding analysis can be easily performed using the described methods.

ACKNOWLEDGEMENTS

We would like to thank Dr. M. Bowler (4GLS) and Dr. P. Dumas (SOLEIL) for precious help in benchmarking and reviewing wavefront propagation functions of SRW.

REFERENCES

[1] C. Pellegrini, S. Reiche, in *Optics Encyclopedia*, Wiley-VCH Verlag, Berlin 2003, p. 1111-1134.
 [2] A. Zholents, W. Fawley, *Phys. Rev. Lett.* 92, 224801 (2004).

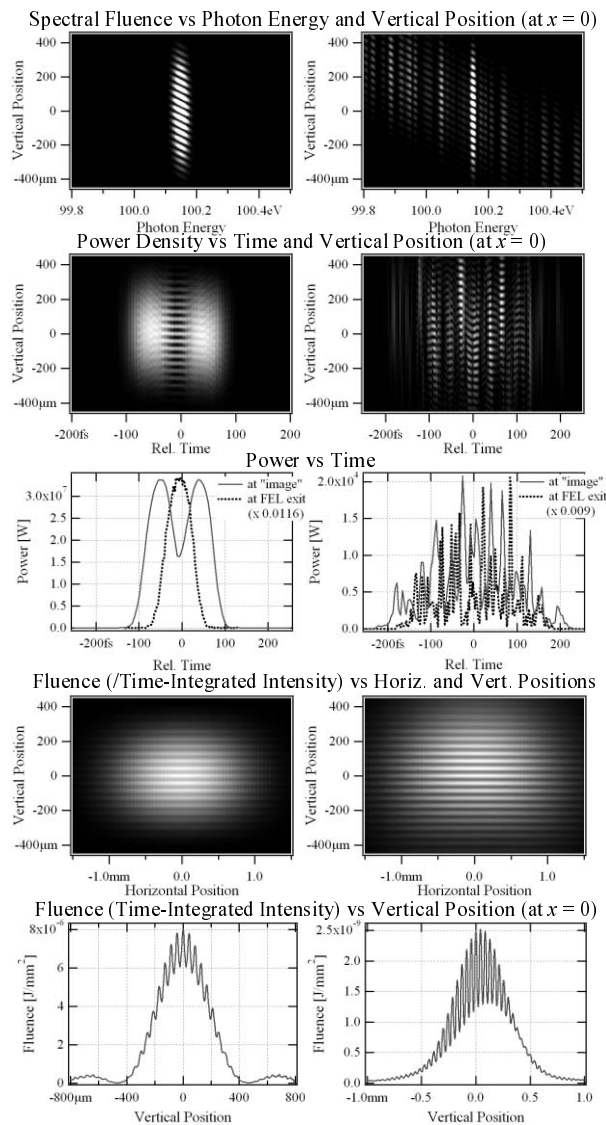


Figure 5: Wavefront characteristics in observation plane of double-slit interferometer with grating, for two FEL regimes: seeded (left) and started up from noise (right).

[3] K.-J. Kim, *Nucl. Instr. and Meth.* A246 (1986) p.71-76.
 [4] K.-J. Kim, *Synchr. Rad. News*, Vol. 19 (6), Dec. 2006, p. 2-6.
 [5] A. Snigirev et. al., *Nature* 384 (1996) p.49.
 [6] M. Hart, L. Berman, *Acta Cryst.* A54 (1998) p. 850-858.
 [7] E. Di Fabrizio et. al., *Nature* 401 (1999) p. 895-898.
 [8] J.W. Goodman, *Introduction to Fourier Optics*, 2nd ed., McGraw-Hill, 1996.
 [9] J. Bahrtdt, *Applied Optics* 36 (19) 1997, p. 4367.
 [10] J. Bahrtdt, *Phys. Rev. ST - Acc. and Beams* 10, 060701 (2007).
 [11] O. Chubar, P. Elleaume, *Proc. EPAC-98*, p.1177-1179.
 [12] O. Chubar et. al., *Proc. SPIE Vol. 4769* (2002) p. 145-151.
 [13] S. Reiche, <http://corona.physics.ucla.edu/~reiche/>.
 [14] M. Born, E. Wolf, *Principles of Optics*, 4th ed., Pergamon Press, 1970.
 [15] S.C. Chan and K.L. Ho, *IEEE Trans. Circuits and Systems* 38 (8), 1991, p. 951-953.
 [16] M.-E. Couprie et. al., these proceedings.
 [17] Z. Chang et al, *Phys. Rev. Lett.* 79 (16) 1997, p. 2967.